Available online at www.sciencedirect.com
SCIENCE DIRECT®
Catalysis Today 88 (2003) 49–59
CATALYSIS TODAY
www.elsevier.com/locate/cattod

Interaction of anatase and rutile TiO_2 particles in aqueous photooxidation

Bo Sun, Panagiotis G. Smirniotis*

Chemical and Materials Engineering Department, University of Cincinnati, Cincinnati, OH 45221-0012, USA

Abstract

The interaction of anatase and rutile titanias was studied with various combinations of TiO_2 catalysts having different particle sizes and impurity contents by photodecomposition of phenol and formic acid. The reactivity of commercial Ishihara ST-series anatase titanias (95% TiO_2) increased with the increase of primary particle size (ST-01, 7 nm; ST-21, 20 nm; ST-41, 200 nm) and the decrease of surface area. Light extinction coefficients of the ST-series anatase TiO_2's at the wavelength of 365 nm were about 1 order of magnitude lower than that of Kemira (KE) rutile TiO_2 having a surface area of 52 m^2/g. Different interactions between anatase and rutile titanias were observed with the mixtures of the ST-series anatase TiO_2's and KE rutile TiO_2. When the irradiation field was dominated by the KE in the mixtures, these interactions inverted completely the order of activities of the ST-series catalysts in phenol photooxidation. The impurity distribution in particles of the Ishihara ST-series TiO_2 catalysts was proposed to explain the above phenomena. The different interactions between anatase and rutile TiO_2 particles were related to their relative Fermi levels prior to their contacting each other. Different interactions between Hombikat UV-100 anatase TiO_2 (HK, 99% TiO_2) and rutile-phase TiO_2 made from HK (HK_R) by heating were observed in phenol and formic acid photodegradations. The change of interaction between HK and HK_R was explained by the stronger hydrolyzation and weaker agglomeration of TiO_2 particles at lower pH values. The experiments done showed that the synergistic effect between anatase and rutile in Degussa P25 was not universal and it was related to the relative Fermi levels of anatase and rutile particles and the particle shape.

Keywords: Charge separation; Photocatalysis; Synergy; Total organic carbon removal; Degussa P25; Band structure

1. Introduction

TiO_2 is known to be the most suitable photocatalyst in the photodegradation of toxic organic molecules for its high activity, nontoxicity and chemical inertness [1–3]. Anatase and rutile [4] are two of TiO_2's forms being frequently studied. TiO_2 of rutile form is claimed as a catalytically inactive or much less active form. However, Degussa P25, which has both anatase and rutile forms with the ratio of anatase to rutile equal to 3–4:1, is one of the best TiO_2 photocatalysts and used frequently as a benchmark in photocatalysis. Bickley et al. [5] developed an anatase and rutile model for the Degussa P25 based on TEM studies. Recent morphology studies showed that the anatase and rutile TiO_2 particles exist separately in the Degussa P25 [6]. Ohno et al. [7] proved the existence of the synergistic effect between contacting anatase and rutile particles. The primary particles in the Degussa P25 are tightly agglomerated in aqueous solutions and the efficient electron transfer through the agglomerates was indicated by the way that

* Corresponding author. Tel.: +1-513-556-1474; fax: +1-513-556-3473.
E-mail address: panagiotis.smirniotis@uc.edu (P.G. Smirniotis).

0920-5861/$ – see front matter © 2003 Elsevier B.V. All rights reserved.
doi:10.1016/j.cattod.2003.08.006

copper particles grow on the Degussa P25 [8]. Sun et al. [9] came up with a band structure of anatase and rutile in Degussa P25 based on their study of platinized TiO_2. It has been shown in numerous studies that there is a positive interaction of anatase and rutile TiO_2 particles of Degussa P25, which enhances the electron–hole separation and increases the total photoefficiency.

Positive interactions were also observed between the anatase and rutile forms of TiO_2 in other systems [7,10,11], and charge separations and synergistic effects between TiO_2 and other substances were reported [12–15]. However, it is still not clear about the exact conditions for the synergistic phenomena occurring in anatase and rutile TiO_2 systems. This study is intended to learn the conditions for the synergistic effect using photooxidation of phenol and formic acid. The experiments showed that the synergistic effect between anatase and rutile TiO_2 that was observed in Degussa P25 was not universal and the effect was related to the relative Fermi levels of anatase and rutile particles and the shape of the particle.

2. Experimental

2.1. Materials and characterizations

The catalysts utilized for studying the anatase and rutile TiO_2 system in the present study (Table 1) were made from commercial titania powders, Hombikat UV-100 (HK, anatase), ST-01, ST-21 and ST-41 (anatase) from Ishihara Sangyo Co. and Kemira UV-TITAN L581 (KE, rutile). Other variations of rutile were made by heating HK and ST-01 in oxygen for 12 h at 1000 °C [16], they were denoted as HK_R and ST-01_R in this study. The BET surface area of the catalysts was measured on Gemini instrument (Micromeritics) at 77 K using liquid nitrogen. Crystalline structures of catalysts were characterized using Nicolet powder X-ray diffractometer equipped with a Cu Kα source. The 2θ was varied in the range from 20° to 50° to assess TiO_2 forms. The absorption and extinction coefficients of the commercial catalysts at the wavelength of 365 nm were determined on a Shimazu 2501PC spectrophotometer with an ISR 2200 integrating sphere attachment [17]. Phenol (Fisher) and formic acid (Fisher, 88%) were used to test catalysts' photoactivities.

2.2. Photocatalytic experiments

The suspension for reaction was prepared by dispersing ultrasonically the mixture of a certain amount of catalyst (dried 6 h at 100 °C before use) with a certain composition (Table 2), 0.065 g phenol or 0.0065 mol formic acid, and 650 ml distilled water for half an hour in an ultrasonic bath (Elma, Ultrasonic LC20H) and stirring the suspension for half an hour afterwards. Careful measurements we performed showed that phenol was not removed from suspension during this procedure.

The photocatalytic oxidation of phenol and formic acid in catalyst suspensions was carried out in a 445 mm long 64 mm in outer diameter annular borosilicate vessel (Ace Glass) with a quartz immersion well

Table 1
Photocatalysts used in the present study

Catalyst	BET surface area[a] (m^2/g)	TiO_2 (%)[b]	Form[c]	Primary particle size (nm)	Extinction coefficient[e] (l/(cm g))	Scattering albedo ω[e]
HK	334	99	Anatase	<10[b]	3.91	0.441
ST-01	217	95	Anatase	7[b]	2.83	0.554
ST-21	69	95	Anatase	20[b]	1.37	0.334
ST-41	11	95	Anatase	200[b]	3.08	0.249
KE	52	99	Rutile	25[d]	24.56	0.472
HK_R	3.6	–	Rutile	–	–	–
ST-01_R	0.35	–	Rutile	–	–	–

[a] Measured on Gemini instrument (Micromeritics) at 77 K.
[b] From manufacture's specifications.
[c] Characterized by XRD (Fig. 1).
[d] Equivalent diameter calculated with the BET surface area.
[e] Measured spectrophotometrically on Shimazu 2501PC UV-Vis with ISR 2200 integrating sphere at the wavelength of 365 nm.

Table 2
Compositions of the catalysts in each experiment and the reaction rates

No.	Anatase	Rutile	Reactant[a]	Reaction rate[b] (mg carbon/(min l))	Maximum light intensity[c] ($\times 10^{-2}$ W/cm^2)
1	0.0650 g HK	0	Phenol	0.069 ± 0.001	3.64
2	0.0650 g HK	0.0072 g KE	Phenol	0.071 ± 0.002	3.54
3	0.0650 g HK	0.0163 g HK_R	Phenol	0.076 ± 0.002	3.50
4	0.0650 g ST-01	0	Phenol	0.057 ± 0.002	4.16
5	0.0650 g ST-01	0.0072 g KE	Phenol	0.062 ± 0.002	3.85
6	0.0650 g ST-01	0.0163 g ST-01_R	Phenol	0.047 ± 0.003	4.12
7	0.0650 g ST-21	0	Phenol	0.061 ± 0.003	4.35
8	0.0650 g ST-21	0.0072 g KE	Phenol	0.059 ± 0.003	3.86
9	0.0650 g ST-41	0	Phenol	0.086 ± 0.007	3.30
10	0.0650 g ST-41	0.0072 g KE	Phenol	0.071 ± 0.002	3.24
11	0.0650 g HK	0	Formic acid	0.355 ± 0.003	3.70
12	0.0650 g HK	0.0163 g HK_R	Formic acid	0.322 ± 0.004	3.52

[a] Initial reactant concentration: 100 mg/l phenol, 10 mM formic acid.
[b] The total organic carbon curves in decompositions of both phenol and formic acid follow zero-order decay kinetics.
[c] The light intensity on the outer wall of the reactor.

(Ace Glass, 49 mm o.d., 7854-27). The UV radiation source was a 450 W medium-pressure mercury vapor quartz lamp (Jelight, J05PM1HGC2). A Pyrex filter (Ace glass, no. 7740) filtered out the far- and mid-UV bands ($\lambda < 320$ nm) of the lamp emission spectrum. The cooling water flowing through the double-walled immersion well eliminated the infrared spectrum of the light. The local light intensities at different locations along the outer wall of the reactor and the outer wall of the cooling jacket were measured for each catalyst with a detector (International Light Inc., Model SED033 #3435) connected to a radiometer (International Light Inc., Model IL 1700). The suspension temperature was maintained at 18.5 ± 0.5 °C. The length of reaction zone was adjusted to 115 mm using aluminum foil on the Pyrex filter and black electric tape on the outer wall of the cooling jacket [18]. The lamp was preheated for 5 min before each experiment for obviating the poor irradiation of the lamp in the first several minutes. The suspension was stirred magnetically and 500 ml/min of oxygen was sparged into the solution from a gas distributor near the bottom of the reactor. The samples (5 ml) of reaction suspension were collected with a syringe at different intervals and filtered with Cameo 25P polypropylene syringe filters (OSMONICS, Cat. #DDP02T2550). At the same time, 5 ml original suspension was added to keep the volume of suspension in the reactor constant. The sample solutions were analyzed with a total organic carbon Analyzer (TOC-VCSH, Shimadzu). Several samples were also analyzed with GC–MS (Shimadzu QP5050A) to identify stable intermediate products.

Mixture of the commercial anatase and rutile TiO_2 prepared at a concentration of 0.25 g/l were tested with a bulk reactor used for earlier studies [9]. The catalysts included the mixtures of the commercial TiO_2 of KE with HK, ST-01, ST-21, or ST-41. The reaction temperature was maintained at 12.5 ± 1 °C. Samples were taken and measured in the same way as above.

3. Results and discussions

3.1. Characteristics of catalysts

The crystalline forms of all titanias used in the present study were determined using X-ray diffraction analysis (Fig. 1). HK, ST-01, ST-21 and ST-41 were anatase form and KE was confirmed to be rutile form, which were consistent with the manufacturers' specifications. The BET surface areas of the commercial catalysts were shown in Table 1. KE was chosen as rutile source because its BET surface area was close to that of Degussa P25 (P25). The surface areas of HK_R and ST-01_R were 3.6 and 0.35 m^2/g, respectively. The much lower surface area of ST-01_R was speculated to be related to the 5% impurity content in this catalyst, which could decrease the energy barrier

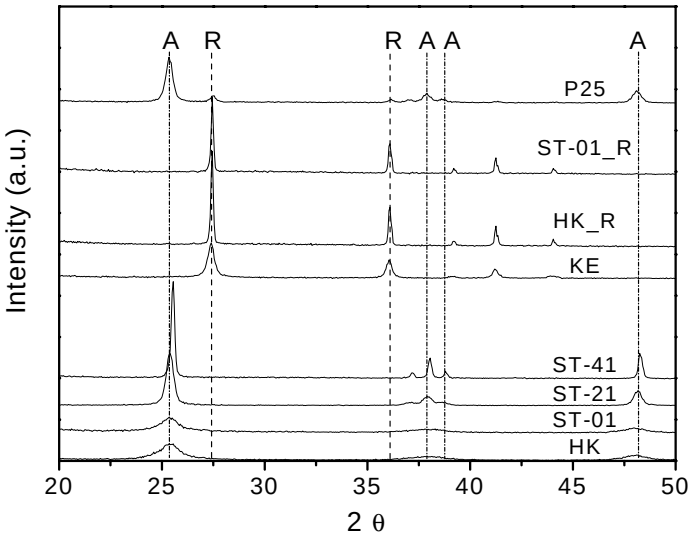

Fig. 1. XRD of the catalysts used in this study A: Anatase, B: Rutile.

between particles for particle agglomeration during heating. The primary particle sizes of ST-01, ST-21, ST-41 were 7, 20 and 200 nm, respectively. The scattering albedo of the ST catalysts changed inversely proportional with their increasing size, which was consistent with the theory of Rayleigh and Mie scattering.

3.2. Irradiation field

For a homogeneous irradiation field and to obtain the intrinsic activities of the catalysts, a reaction zone with a small annular gap and a short length was used. The annular gap in this study was 6 mm and the length was 115 mm. The uniformity of the light in the reaction zone is also highly dependent on the catalyst's optical characteristics and concentration (Table 1). The extinction coefficients of anatase TiO_2's were about 1 order of magnitude lower than that of KE rutile. Beer–Lambert law was used to simulate the light intensity in the reaction zone with the measured inner and outer wall light intensities. The light intensity measurements were done on the outer wall with the different commercial catalysts (Table 2). The measurements indicated the influence of nonuniform irradiation field resulted from the light absorption and scattering by the particles in the reaction suspension. The light intensities measured with pure anatase TiO_2 suspension (Table 2) showed that the light intensity decreases as the extinction coefficient (Table 1) increases. The decrease of the light intensity on the outer wall after the addition of the same concentration of KE TiO_2 was smaller for the anatase catalyst with a larger extinction coefficient. This is consistent with KE's extinction coefficient being higher than all the anatase catalysts.

3.3. Performances of the anatase titanias

The total organic carbon concentration curves in phenol decomposition with the different commercial anatase TiO_2 catalysts (0.1 g/l) in the first reactor are shown in Fig. 2. The TOC concentration decreased linearly with time, which complied with earlier studies [9]. Results of reaction with these and other catalysts using the differential reactor are summarized in Table 2. It was interesting to see that the reaction rates did not decrease with increase of the primary particle size of the ST-series catalyst as the rates increased from 0.057, 0.061, to 0.086 mg carbon/(min l) for ST-01, ST-21, and ST-41 separately. The reactivity of ST-41 was higher than that of HK TiO_2 (0.069 mg carbon/(min l)), which indicated an effective charge separation inside ST-41 particles. The BET surface areas of ST-01, ST-21, and ST-41 were 217, 69, and 11 m^2/g, respectively (Table 1). Therefore, the lower

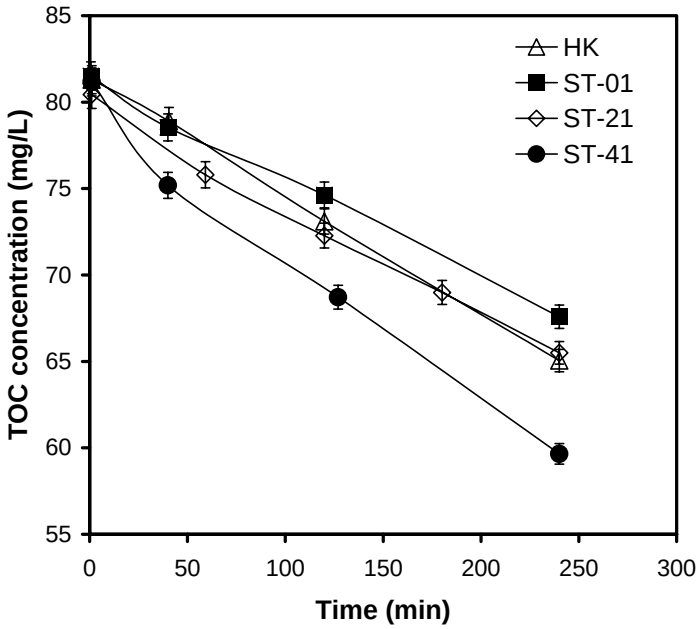

Fig. 2. The degradation of total organic carbon (TOC) as a function of time for HK, ST-01, ST-21, and ST-41 during phenol photooxidation. Catalyst concentration: 0.1 g/l; initial pH: 6.97; reaction temperature: $18.5 \pm 0.5\,^{\circ}C$.

surface area and larger particle size of the particle did not necessarily result in a higher electron–hole recombination rate and lower charge transfer. Earlier studies [19] indicated that this phenomenon may not be observed with pure anatase. The results imply that number of active sites on the surface brought about by the impurities increases as the surface area of the ST-series catalysts decreases. The TiO_2 in ST-41 is 95% based on the manufacturer's specification. It can be seen from the study of Cr-implanted TiO_2 [20] uniform distribution of the impurity in a TiO_2 particle cannot bring a good charge separation. Therefore, there should be an impurity gradient across the particle radius in the ST-41 particle, which may be formed during crystallization. The pure TiO_2, which had the highest melting point, first crystallized, forming a core. The more impure TiO_2 crystallized later and enclosed the purer TiO_2 inside. In the end, ST-41 particle formed with a TiO_2 purity changing from the highest at the center of the particle to the lowest at the edge of the particle. The possible n- and p-type band structures brought about by the nonuniform impurity distribution [21] were schematically shown in Fig. 3. In either type, electrons and holes created tend to move in the opposite directions under the force of electrical potential field [21] and the charge separation inside the particle is improved. ST-01 and ST-21 may not have the nonuniform impurity distribution as ST-41 has because particles of smaller sizes need a shorter crystallization time and the impurities are more probable to condense at the same time of TiO_2 crystallization.

3.4. Effects of impurities on interaction between anatase and rutile TiO_2

Different effects of changes in reaction rates were observed before and after the addition of KE with ST-01 and ST-41 (Table 2). The TOC removal rate for ST-01 increased by 9% with the addition of 10% KE, while that for ST-41 decreased by 17%. The KE addition did not have a significant effect on the rate for ST-21. Therefore, the data suggests that the interaction of anatase and rutile particles was related to the particle size and the surface area of the catalyst. ST-21's surface area was 69 m^2/g and its particle size was 20 nm, both of which were very close to those of P25. Therefore, the surface area and particle size of P25 cannot prove it to be an efficient catalyst. The

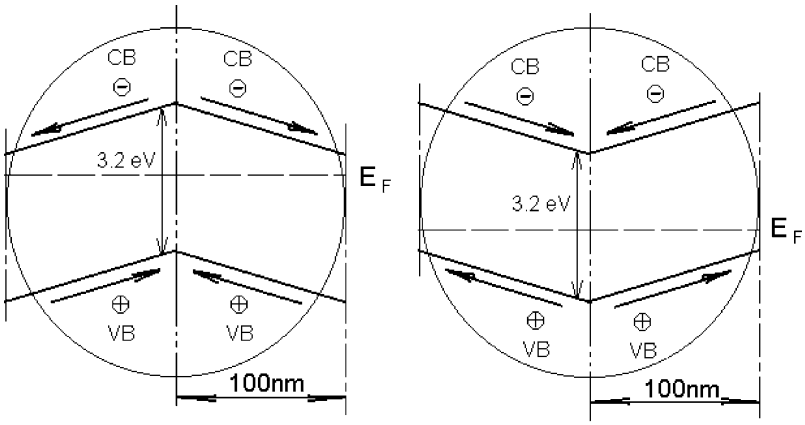

Fig. 3. Schematic drawing of n-type (a) and p-type (b) band structure of ST-41. The linear relation drawn between the band energy and radius is just for simplicity and it need not be linear, it depends on the impurity concentration at different radii.

proposed P25's band structure [9] can also be used to illustrate the interaction between HK and KE, ST-01 and KE in the agglomerates [8]. The suggested model for the interaction between the ST-41 anatase and KE rutile was illustrated with the band structure after Fermi level lineup in Fig. 4 [21]. In Fig. 4a, a part of holes created in ST-41 anatase TiO_2 particles can flow into KE rutile TiO_2 particles under the force of potential gradient, but the electrons cannot. Thus, the charge recombination in anatase can be decreased. However, the impurity concentration at the edge of ST-41 particles can be much higher than 5% because of the nonuniform impurity distribution, which may bring about energy degradation [22]. And this can be the reason for the negative interaction between ST-41 and KE. In comparison, ST-01 and ST-21 do not suffer as much energy degradation as ST-41 does due to their much more uniform impurity distributions. In Fig. 4b, the Fermi level of p-type anatase TiO_2 is lower than that of rutile TiO_2. Electrons in ST-41 tend to flow into KE and holes in KE tend to go in the opposite direction. But since rutile TiO_2 is nearly inactive, electrons and holes in KE rutile TiO_2 recombine with each other. Finally, the transfer of electrons and holes across the interface between particles will stop in order to keep the neutrality of the particles. The KE rutile particles being in contact with ST particles may reduce the active sites on the surface of ST-series particles. And because the surface area of ST-41 is much smaller than those of ST-01 and ST-21, the activity of ST-41 decreases the most after the addition of KE.

The addition of ST-01_R to ST-01 decreased the TOC decomposition rate by 18% (Table 2), which differed from the 9% increase brought about by the addition of KE. Since the light intensity change brought about by the addition of ST-01_R was negligible, the decrease was attributed to the negative interaction between ST-01 and ST-01_R. Anatase TiO_2 is 9% less dense than rutile TiO_2 [23]. Hence, ST-01 TiO_2 became denser during the process of conversion from anatase to rutile. At the same time, the impurity concentration inside the particle became larger, which could bring about a small change in Fermi level [21]. The results indicated the effect of relative Fermi levels between anatase and rutile on their interaction.

All the anatases used in this study had a much smaller extinction coefficient than KE rutile and P25 [17], and the extinction coefficient of KE was similar to that of P25, so it was reasonable to assume that the light extinction by P25 at 365 nm was mainly caused by the rutile phase. The anatase and rutile particles in P25 were formed at the same time by high temperature hydrolysis of $TiCl_4$ and it was more than 99.5% pure [24]. The types and concentrations of impurities and Fermi level in anatase of P25 are expected to be similar to those in rutile. These facts and the above discussions imply that one of the reasons for P25's high activity can be the appropriate relative Fermi

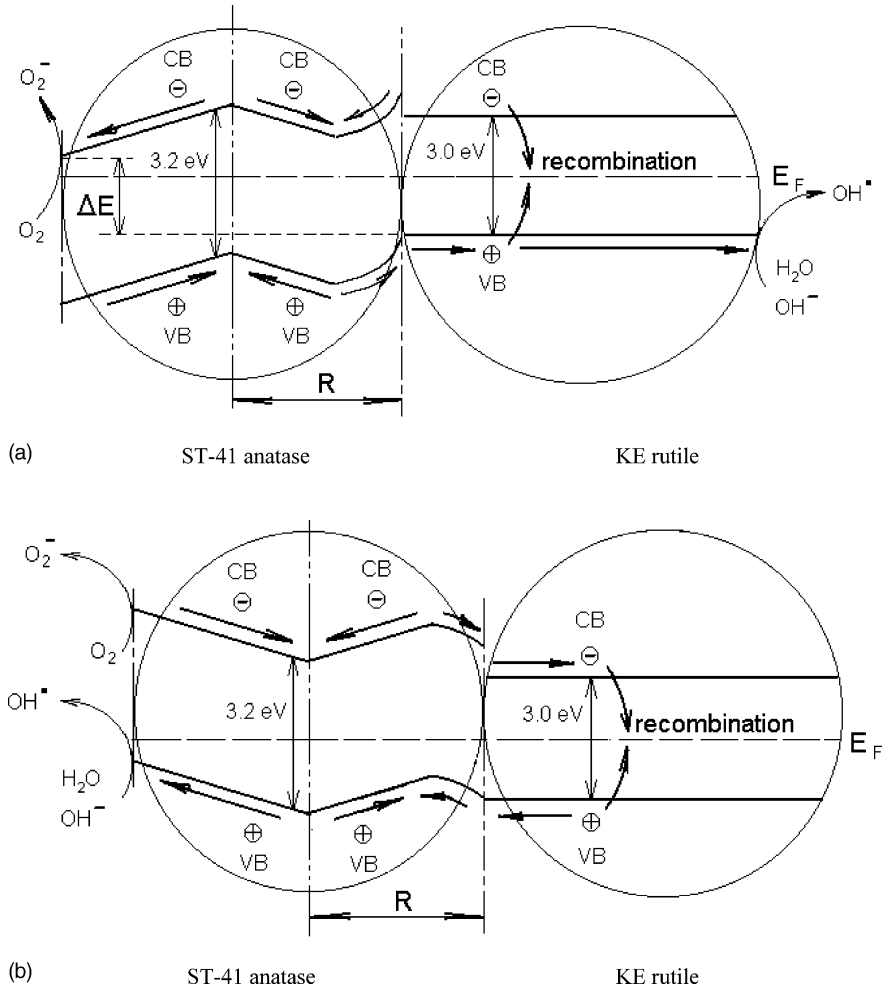

Fig. 4. Schematic drawing of proposed band structure of ST-41 anatase and KE rutile particles in contact after Fermi level lineup: (a) and (b) are drawn according to the n- and p-type structures in Fig. 3.

levels between anatase and rutile TiO_2's prior to their contacting each other, which can help charge separation [9,25]. The other interesting aspect of P25 is that its particles are cubic with round edges [5,24]. These anatase and rutile TiO_2 particles being in contact have a much larger interface area than spherical particles, enhancing the synergy.

3.5. Effects of pH and agglomeration on interaction between anatase and rutile TiO_2

The TOC concentration curves during phenol and formic acid photodecomposition with the mixture of HK and HK_R are shown in Fig. 5. The addition of 20% HK_R increased the TOC removal rate in phenol degradation by 10%, while it decreased that in formic acid degradation by 9%. The pH of 0.1 g/l phenol suspension was 6.97 and the pH of 10 mM formic acid suspension was 2.95. The observation imply that the decrease in pH can decrease the interaction of HK and HK_R, which is consistent with earlier studies with P25 [26]. The pH cannot change the difference in band potential [27] between anatase and rutile TiO_2 because they are in the same solution. The particles exist in agglomerates in solution [7,8]. Particle agglomeration in solution is caused by the Van der Waals

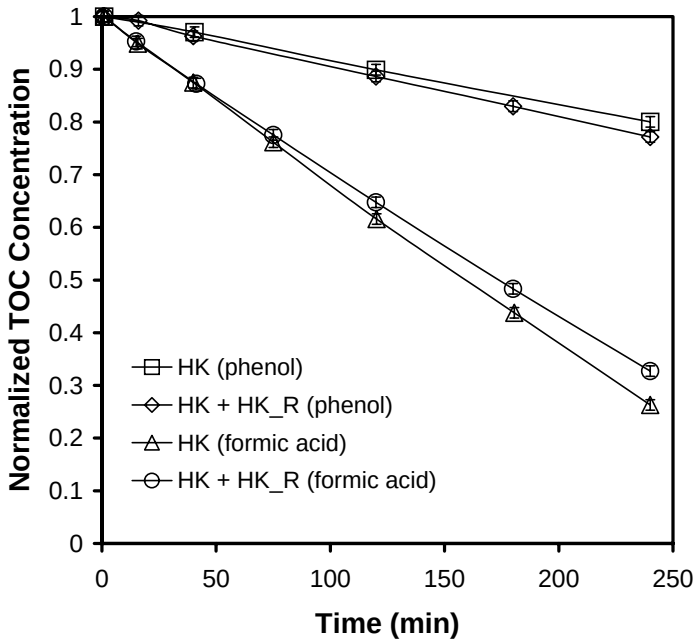

Fig. 5. Normalized total organic carbon (TOC) concentration as a function of time for HK and HK_R in phenol and formic acid photooxidation. HK concentration: 0.1 g/l; HK_R concentration: 0.025 g/l; initial reactant concentration: 100 mg/l (phenol), 10 mM (formic acid); initial pH: 6.97 (phenol suspension), 2.95 (formic acid suspension); reaction temperature: $18.5 \pm 0.5\,^{\circ}C$.

forces (attractive) and electrostatic forces (repulsive) [28], which can be affected by hydrolyzation of TiO_2 surface [1]. Since more hydrolyzation of TiO_2 surface occurs at lower pH, that brings larger repulsive forces between the particles. The agglomeration and interaction between the anatase and rutile TiO_2 particles weaken at lower pH. Therefore, the pH can affect the interaction of anatase and rutile TiO_2's and their photoactivity. Agglomeration cannot happen if the particle size was very big [29]. It can occur in the catalysts used in the present study since the sizes of the catalyst particles were small. The agglomeration is shown to be an important factor for the catalyst's photoactivity.

3.6. Study with the bulk reactor

Fig. 6a shows the relation of the anatase content to the activities of anatase and rutile TiO_2 mixture in phenol photodegradation with the second reactor [9]. The corresponding curves of normalized TOC removal rate are shown in Fig. 6b. Different trends were observed with HK and the ST-series catalysts. The TOC removal rate increased almost linearly with increasing HK content. Pure KE, which is rutile form TiO_2, was nearly inactive compared with the tested anatase catalysts. The reaction rate with pure HK was the lowest among those with pure anatase catalysts. However, the reaction rate with the mixture of HK and KE was the highest when the anatase content was less than 70%. The activity of ST-41 was the lowest (Fig. 6a) and was reduced the most (Fig. 6b) when the anatase content was less than 70%.

The photocatalytic decomposition of phenol was related to the irradiation field and the intrinsic activity of the catalysts. When the KE rutile content was low, the rank of the reaction rates with different catalysts was as follows: ST-41 $\approx$ ST-21 > ST-01 > HK. The highest reaction rate with ST-41 can be explained by its highest intrinsic activity among the anatase titanias. The lowest reaction rate of HK implied the influence of the irradiation field. The extinction coefficient with HK was the highest among the anatase titanias used (Table 1). The light intensity was the most nonuniform in the HK suspension, and decreased the most

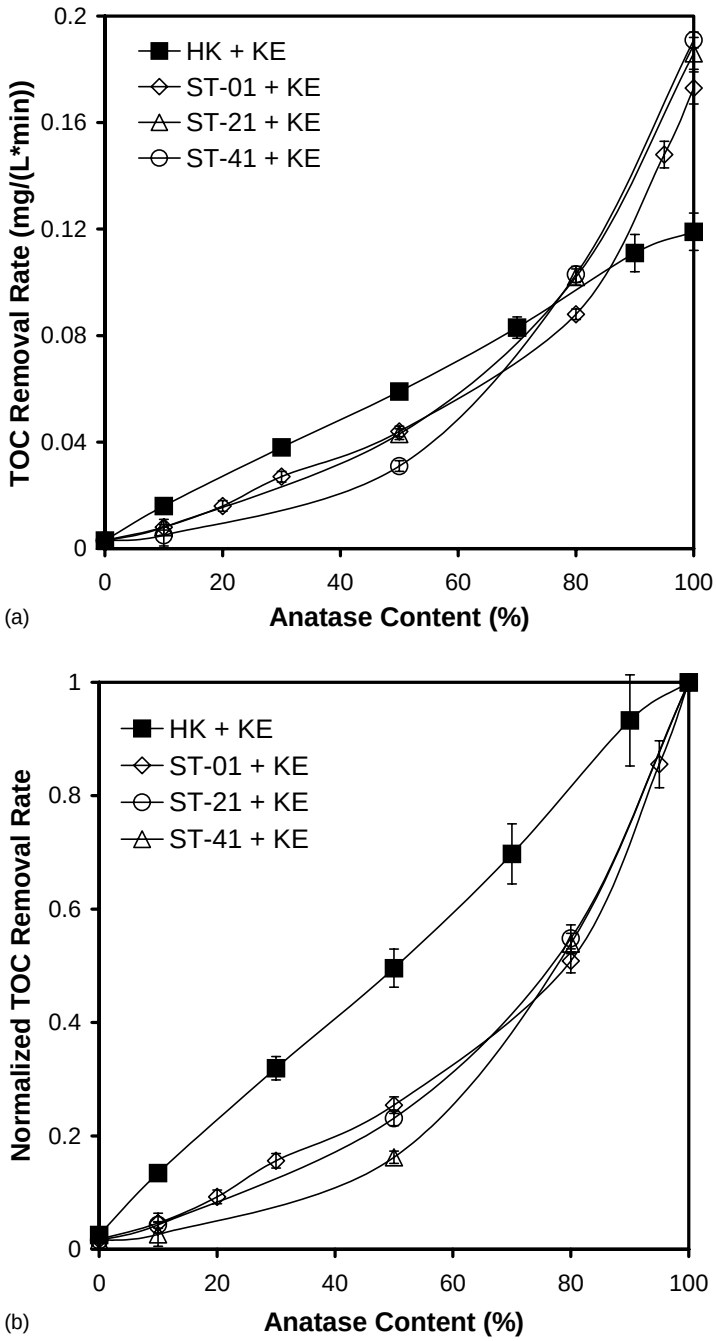

Fig. 6. (a) The total organic carbon (TOC) removal rates with mixtures of HK and KE, ST-01 and KE, ST-21 and KE, ST-41 and KE during phenol photooxidation. Initial pH: 6.97; reaction temperature: $12.5 \pm 1\,^{\circ}$C. (b) Normalized total organic carbon (TOC) removal rates with mixtures of HK and KE, ST-01 and KE, ST-21 and KE, ST-41 and KE during phenol photooxidation. Initial pH: 6.97; reaction temperature: $12.5 \pm 1\,^{\circ}$C.

from the inner wall to the outer wall of the reactor zone. The positive interaction found above between HK and KE can just counteract the unfavorable irradiation field brought by adding KE rutile. When the KE content was high, the irradiation field was dominated by the existence of KE because of its much higher extinction coefficient, and corresponding reaction rates was ranked in order from the highest to the lowest: HK > ST-01 ≈ ST-21 > ST-41. The rank of the ST-series catalysts is consistent with the order of interaction of ST-series catalysts and KE learned above with the first reactor. The positive interaction between HK and KE and HK's higher reactivity compared with ST-01's ensured that the mixture of HK and KE had the highest reactivity when KE content was high.

3.7. Reaction intermediates

We observed color change in the solution during phenol photocatalytic degradation. After irradiation, the originally transparent solution turned into rose gradually first and then it turned back to transparent again. Such intensive discoloration precluded the use of UV-Vis spectroscopy for quantification of phenol in solution. We detected volatile and semivolatile compounds in the solution using GC–MS technique. Direct injection of the solution into the GC–MS did not provide any significant peaks of volatile compounds suggesting that their concentration was very low. To detect semivolatiles derivatization with a trimethylsilyl reagent was used that transformed polar compounds into their volatile trimethylsilyl derivatives. The main two peaks corresponded to hydroquinone and catechol. Resorcinol and various acids were formed as a result of phenyl ring opening. These compounds are mostly bi-functional alkanoic and alkenoic acids and hydroxylated acids such as hydroxyacetic acid. Hydroquinone and catechol were detected as products of phenol photocatalytic oxidation over TiO_2 Hombikat and P25 previously [30]. Benzoquinone was also detected in phenol photocatalytic oxidation as it is easily formed because of hydroquinone oxidation by oxygen. Hydroquinone and benzoquinone can form a rose semiquinone complex. Therefore, rose discoloration during phenol photocatalytic oxidation is most probably related to light absorption by hydroquinone–benzoquinone complex.

4. Conclusions

The intrinsic photoactivities of pure anatase TiO_2 catalysts in the study followed ST-41 > HK > ST-21 > ST-01. The increase in activity of the ST-series anatase TiO_2 with particle size increasing was related to the impurity distribution in particles of the catalysts. The interaction between ST-01 anatase TiO_2 and KE rutile TiO_2 was positive and that between ST-41 and KE was negative, the interaction between ST-21 and KE was in the middle. These interactions changed completely the order of activities of pure ST-series catalysts in phenol photooxidation to the converse when the percentage of KE was high in the mixture of ST-series catalyst and KE. The interactions between anatase and rutile titanias depended on pH and their relative Fermi levels. Agglomeration was one of the conditions for the anatase and rutile titanias to interact and it happened among small particles. The photoactivity of a catalyst was affected by the nonuniform irradiation field. The synergistic effect between anatase and rutile observed in Degussa P25 was not universal and it was related to the relative Fermi levels of anatase and rutile TiO_2 particles prior to their contacting each other and the particle shape.

Acknowledgements

The authors wish to acknowledge the NSF and the US Department of Army for partial support for this work through the grants CTS-0097347 and DAAD 19-00-1-0399, respectively. We also acknowledge funding from the Ohio Board of Regents (OBR) that provided matching funds for equipment to the NSF CTS-9619392 grant through the OBR Action Fund #333.

References

[1] M.R. Hoffman, S.T. Martin, W.Y. Choi, D.W. Bahnemann, Chem. Rev. 95 (1995) 69.
[2] M.A. Fox, M.T. Dulay, Chem. Rev. 93 (1993) 341.
[3] A.L. Linsebigler, G. Lu, J.T. Yates, Chem. Rev. 95 (1995) 735.
[4] L. Kavan, M. Gratzel, S.E. Gilbert, C. Klemenz, H.J. Scheel, J. Am. Chem. Soc. 118 (1996) 6716.
[5] R.I. Bickley, T. Gonzalez-Carreno, J.S. Lees, L. Palmisano, R.J.D. Tilley, J. Solid State Chem. 92 (1991) 178.

[6] A.K. Datye, G. Riegel, J.R. Bolton, M. Huang, M.R. Prairie, J. Solid State Chem. 115 (1995) 236.
[7] T. Ohno, K. Jarukawa, K. Tokieda, M. Matsumura, J. Catal. 203 (2001) 82.
[8] S.J. Kim, E.G. Lee, S.D. Park, C.J. Jeon, Y.H. Cho, C.K. Rhee, W.W. Kim, J. Sol–Gel Sci. Technol. 22 (2001) 63; K.R. Lee, S.J. Kim, J.S. Song, J.H. Lee, Y.J. Chung, S. Park, J. Am. Ceram. Soc. 85 (2000) 341.
[9] B. Sun, A.V. Vorontsov, P.G. Smirniotis, Langmuir 19 (2003) 3151.
[10] R.R. Bacsa, J. Kiwi, Appl. Catal. B Environ. 16 (1998) 19.
[11] K. Tanaka, M.F.V. Capule, T. Hisanaga, Chem. Phys. Lett. 187 (1991) 73.
[12] G. Blondeel, A. Harriman, D. Williams, Solar Energy Mater. 9 (1983) 217.
[13] H. Tada, A. Hattori, Y. Tokihisa, K. Imai, N. Tohge, S. Ito, J. Phys. Chem. B 104 (2000) 4585.
[14] T. Kawahara, Y. Konishi, H. Tada, N. Tohge, S. Ito, Langmuir 17 (2001) 7442.
[15] F. Ye, A. Ohmori, Surf. Coat. Technol. 160 (2002) 62.
[16] S. Nishimoto, B. Ohtani, H. Kajiwara, T. Kagiya, J. Chem. Soc., Faraday Trans. I 79 (1983) 2685.
[17] L. Davydov, P.G. Smirniotis, J. Catal. 191 (2000) 105.
[18] L. Davydov, S.E. Pratsinis, P.G. Smirniotis, Environ. Sci. Technol. 34 (2000) 3435.
[19] M. Gratzel, A.J. Frank, J. Phys. Chem. 86 (1982) 2934.
[20] T. Sumita, T. Yamaki, S. Yamamoto, A. Miyashita, Thin Solid Films 416 (2002) 80.
[21] S.M. Sze, Physics of Semiconductor Devices, Wiley, 1981 (Chapters 1–2).
[22] H.P. Maruska, A.K. Ghosh, Solar Energy 20 (1978) 443.
[23] A. Fahmi, C. Minot, Phys. Rev. B 47 (1993) 47.
[24] D.F. Ollis, H. Al-Ekabi, Photocatalytic Purification and Treatment of Water and Air, Elsevier, Amsterdam, 1993, p. 801.
[25] T. Kawahara, Y. Konishi, H. Tada, N. Tohge, J. Nishii, S. Ito, Angew. Chem. Int. Ed. 41 (2002) 2811.
[26] C. Kormann, D.W. Bahnemann, M.R. Hoffmann, Environ. Sci. Technol. 25 (1991) 494.
[27] M. Gratzel, Heterogeneous Photochemical Electron Transfer, CRC Press, Boca Raton, 1989, p. 106.
[28] A. Mersmann, Crystallization Technology Handbook, Marcel Dekker, New York, 2001, p. 235–281.
[29] T. Ohno, K. Sarukawa, M. Matsumura, New J. Chem. 26 (2002) 1167.
[30] K.I. Okamoto, Y. Yamamoto, H. Tanaka, M. Tanaka, Bull. Chem. Soc. Jpn. 58 (1985) 2015.